COREGISTRATION METHOD FOR ROTATED/SHIFTED FOPEN SAR IMAGES

Luca Pallotta[†], *Carmine Clemente*[*], *Gaetano Giunta*[†], *and John J. Soraghan*[*]

[†] University of Roma Tre, Rome, Italy
[*] University of Strathclyde, Glasgow, UK

ABSTRACT

This paper tests a SAR image coregistration method, developed to account for a joint rotation and range/azimuth shift effect in absence of zooming, on foliage penetrating (FOPEN) data. In particular, the method is referred as a constrained Least Squares (CLS) optimization method and, in its basic form, it sharply extracts all patches composing the entire image. Differently, in next developments it applies a detection stage to identify extended areas in the images where patches are then selected. Moreover, it also performs a refinement of the equations in the CLS problem through an iterative cancellation procedure. The performance of this enhanced version of the CLS are made on the challenging Carabas-II VHF-band FOPEN SAR data to demonstrate its effectiveness also in high-resolution SAR images.

Index Terms— Synthetic Aperture Radar (SAR) coregistration, foliage penetrating (FOPEN), rotation and translation.

1. INTRODUCTION

Multitemporal synthetic aperture radar (SAR) images generally differ each other because of the, even slight, variations in the platform trajectories during acquisition. These mismatches directly reflect on the position of the final scene and, hence, on final SAR-related products. This issue is addressed by using a coregistration procedure [1, 2] that is done after the image formation process, and consists in aligning the slave image on the master. This procedure can follow two competing philosophies: a) feature-based relying on the identification of the tie-points in the images [3–5], and b) area-based, exploiting the misalignment information, for instance, embedded in the spatial cross-correlation [6–8]. In [9], a method for SAR image coregistration in the presence of rotation and translation has been proposed. It improves the performances of the constrained least squares (CLS) method [10] in which the displacement field is build-up from all the patches composing the image. Differently, in [9], the coregistration algorithm performs a pre-processing stage aimed at identifying extended targets/areas within both images. Then, their centroids are considered to be candidate tie-points for the subsequent formulation of the CLS problem. Once the problem is formalized, the set of equations is iteratively refined performing an outlier cancellation procedure in agreement with their absolute error. The scope of this paper is to assess the effectiveness of the CLS of [9] on the challenging high resolution Carabas-II VHF-band FOPEN SAR data [11].

2. PROBLEM FORMULATION

Consider two complex images of the same scene, $\boldsymbol{I}_m(z) \in \mathbb{C}^{K\times N}$ (master) and $\boldsymbol{I}_s(z) \in \mathbb{C}^{K\times N}$ (slave), with $z = x + jy$ the complex variable describing the Cartesian coordinates x and y. The effect of a respective pixels translation and rotation can be defined as

$$\boldsymbol{I}_s(z) = \boldsymbol{I}_m((z-\delta)/\alpha) + \boldsymbol{E}(z), \tag{1}$$

with $\boldsymbol{E}(z)$ the error image accounting for noise and different scattering properties, $\delta = \delta_x + j\delta_y$ the complex displacement, and $\alpha = \gamma\exp(j\theta)$ a scaling factor accounting for rotation (θ) and zooming (γ). Setting $\gamma = 1$ to enforce the absence of zooming effects, the problem consists in estimating the unknown parameters $\delta \in \mathbb{C}$ and $\theta \in \mathbb{R}$. To do this, let us indicate with $\zeta_l = x_{s,l} + jy_{s,l}$, $l = 1, \ldots, L$, the complex valued coordinates position of the ground control points in the slave image and with $z_l = (x_{m,l} + jy_{m,l})$, $l = 1, \ldots, L$, those in the master. Then, the displacement field between them is the solution of a constrained over-determined linear system of L equations in 3 unknowns [9, 10]

$$\begin{cases} \arg\min_{\boldsymbol{p}} \|\boldsymbol{Z}\boldsymbol{p} - \boldsymbol{\zeta}\|^2 \\ \text{s.t. } \boldsymbol{p}^\dagger \boldsymbol{D}\boldsymbol{p} - 1 = 0 \end{cases}, \tag{2}$$

with $\|\cdot\|$ indicating the Euclidean matrix norm and $(\cdot)^\dagger$ the conjugate transpose operators, whereas

$$\boldsymbol{p} = \begin{bmatrix}\alpha \\ \delta\end{bmatrix}, \ \boldsymbol{Z} = \begin{bmatrix} z_1 & 1 \\ \vdots & \vdots \\ z_L & 1 \end{bmatrix}, \ \boldsymbol{D} = \begin{bmatrix}1 & 0 \\ 0 & 0\end{bmatrix}, \text{ and } \boldsymbol{\zeta} = \begin{bmatrix}\zeta_1 \\ \vdots \\ \zeta_L\end{bmatrix},$$

with the coordinates $\zeta_1, \ldots, \zeta_L$ expressed with respect to the reference system centered at the image center.

3. COREGISTRATION ALGORITHM DESCRIPTION

Although in [10] the solution to the CLS problem of (2) is given in closed-form, it has the drawback of considering all

patches composing the images. In fact, it divides the images into a certain number of patches and extracts the ground control points at the positions of the cross-correlation maxima. By doing so, some performance degradations are experienced when some patches share low coherence, when there are noisy patches, or when a poor correlation peak estimate is computed. These limitations are somehow overcame in [9], where two main improvements are brought to the standard CLS, that is:

- the ground control points are selected with a target detection-based approach;
- the set of equations in the CLS is refined rejecting those identified to be outliers.

The main steps involved in the algorithm are summarized in Fig. 1. The algorithm starts with the application of a constant false alarm rate (CFAR) detection scheme to both images to reveal all possible extended strong reflective areas in the scene [12]. Herein, without loss of generality, the classic cell-averaging CFAR (CA-CFAR) is used to obtain the binary detection map. This latter is then further refined during the next steps that comprise a clustering and false alarms cancellation procedure. The clustering is performed former by an order filter that replaces the element of the pixel under test by an element in the sorted set of neighbors to provide a complete shape of the detected object. Then, to remove all isolated detections due to noise spikes or strong reflections associated with point-like targets, a median filter is applied.

The third step estimates the centroid for each extended target computing the center of mass of the detected cluster of pixels. Then, for each centroid in the master, the corresponding in the slave is found as the one sharing the lower Euclidean distance from it. This approach allows the ambiguities in the association process to be resolved. In fact, since the number of detected centroids could be different in the two images, those not associated are directly removed, possibly reducing the number of coupled centroids to $L_1 \leq L$. Now, the tie-points to form the CLS problem of (2) are selected as the centroids' positions in the two images (this method is indicated as C-OBCLS). An alternative version consists in using the peak of the real 2D cross-correlation between the modulus of corresponding patches centered in the detected centroids. This choice is motivated by the fact that some associated detections could not belong to the same target (e.g., a target is present only in one image). In such a case, it would be better to refer to the area surrounding the detected centroids and evaluates the cross-correlation of the patches centered at the centroid position (this is referred as RC-OBCLS).

The last step of the algorithm performs the cancellation of the equations resulting to be outliers within the set composing the CLS. This operation is performed rejecting the equations sharing the highest absolute errors of the estimated parameters vector $\boldsymbol{p}$, that is are defined as

$$\boldsymbol{\epsilon} = [\epsilon_1, \ldots, \epsilon_{L_1}]^T = |\boldsymbol{Z}\hat{\boldsymbol{p}} - \boldsymbol{\zeta}|, \tag{3}$$

where $(\cdot)^T$ denotes the transpose operator and $|\cdot|$ is the modulus of each element in the vector. Precisely, for each absolute error value, ϵ_l, $l = 1, \ldots, L_1$, the equations contained in (2) for which ϵ_l is greater than a specific threshold are removed leading to a new reduced-size CLS problem. The threshold is selected resorting to the median absolute deviation (MAD) criterion [13, 14], that functionally depends on a parameter κ ruling the degree of cancellation. This algorithm is iteratively repeated starting from $\kappa = 3$ to $\kappa = 2$ with a step size of 0.25.

4. PERFORMANCE ASSESSMENT ON FOPEN DATA

This section is aimed at assessing the performance of the proposed methodology on a radar dataset comprising FOPEN SAR images. More precisely, the selected images belong to the Carabas-II VHF-band (20-90 MHz) SAR data collected in northern Sweden in 2002 [11]. The dataset comprises 24 magnitude images of the same observed scene. The annotated images are characterized by the presence of 25 vehicles displaced on terrain and concealed by foliage [11]. Each image has a size of 3000×2000 pixels, where the rows correspond to the north-south direction, whereas the columns correspond to the east-west direction. Moreover, since the pixel size is 1×1 meter, the acquired scene represents a zone of 3×2 km. As to the targets, four deployments are associated with the SAR images, with 25 terrain vehicles of three types. For the following tests, we consider the dataset referred as "*Sigismund experiments*" with the acquisition "$v02\_2\_1\_1.a.Fbp.RFcorr.Geo.Magn$" used as master and that "$v02\_2\_3\_1.a.Fbp.RFcorr.Geo.Magn$" as slave. Since the quoted couple is already registered, in the subsequent analysis the slave is counterclockwise rotated by an angle θ to be then estimated by the proposed algorithm. Moreover, to reduce the overall computation burden, the results refer to images of size 2000×2000 m, as shown for the master in Fig. 2.

Before going into details in conducted tests, in Fig. 3 the centroids of the extended targets after the coupling process between master and slave are illustrated. These are obtained at the output of the CFAR detector, false alarms removing process and detection clustering. Therefore, the displacement field, that is the starting point for the CLS used to estimate the rotation angle θ, is derived.

In order to study the effect of the rotation angle on the effectiveness of the considered registration algorithm, the slave image is counterclockwise rotated by an angle θ varying in the interval $[0°, 4°]$. The performance are investigated using as figure of merit the estimated rotation angle, the estimated displacement, and the RMSE varying the rotation angle in the above described interval. More precisely, Fig. 4 depicts the estimated values of the rotation angle for all rotations applied

Fig. 1. Block scheme of the SAR images coregistration algorithm of [9].

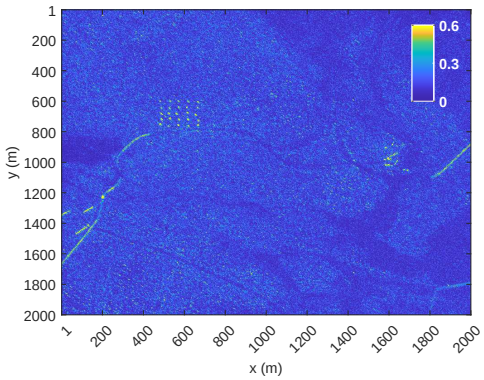

Fig. 2. Carabas-II master image.

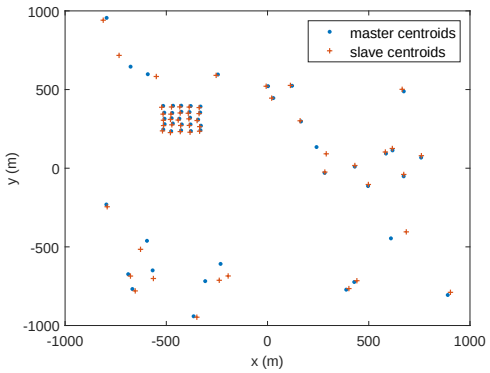

Fig. 3. Centroids detected and coupled for the Carabas-II master and slave images.

to the slave. From a first visual inspection it is quite clear that both the versions of the proposed method are able to correctly estimate the angle up to the value of $2.5°$. Conversely, as the respective rotation angle between master and slave increases, viz. from $3°$ to $4°$, the estimation error is increasing, with a general trend in underestimating the true value. This behavior can be explained by the fact that the induced rotation process on the slave image acts also a re-sampling on the imagery through a nearest neighbor interpolation that, in turn, provides some variations in the scene, with a consequent impact on the overall performances of the algorithm. The final observation of the results shown in Fig. 4 regards the fact that the RC-OBCLS performs slightly better than the C-OBCLS, with the classic CLS that instead completely fails.

To corroborate further with the results shown in Fig. 4 in terms of estimated rotation angle, in Fig. 5 the estimated displacement is reported for each rotation angle. The plotted values confirm the trend observed in the previous graph; in fact, the proposed technique correctly estimates the displacement, which should be very close to 0 pixels since only a rotation has been applied on the slave image. Nevertheless, as seen in Fig. 4, also in Fig. 5 the estimated values are satisfactory for θ from $0°$ to $2.5°$. Then, the estimated displacement tends to grow, overestimating its true value. This result is perfectly in line with the estimated angle since when the algorithm tends to underestimate the rotation angle, the residual values are associated with a pure translation.

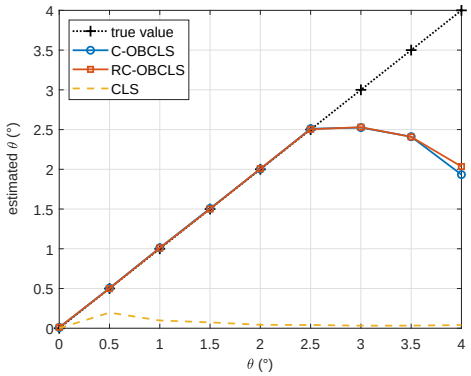

Fig. 4. Estimated rotation angle for Carabas-II SAR images.

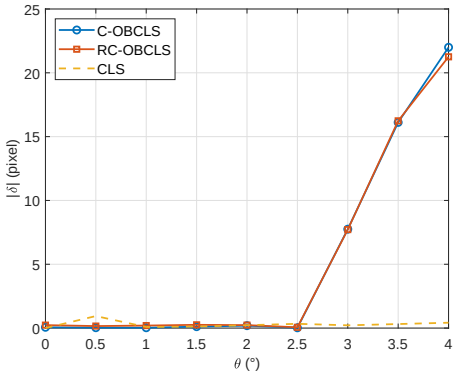

Fig. 5. Estimated displacement (modulus expressed in pixels) for Carabas-II SAR images.

To conclude this study as well as to provide a concise measure of the capability of the proposed algorithm in estimating the rotation and displacement between a couple of images, in Fig. 6, the RMSE of the estimated position vector $\boldsymbol{p}$ is displayed versus the induced rotation angle θ, for the

above illustrated scenario. As expected, the RMSE exactly reflects the same behavior emphasized in the curves of Figs. 4 and 5, with its lower values associated with those of θ less than or equal to $2.5°$.

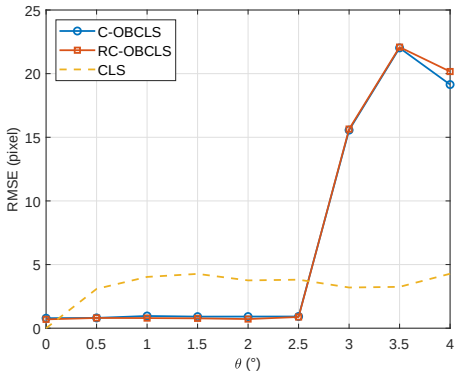

Fig. 6. RMSE (in pixels) for Carabas-II SAR images.

5. CONCLUDING REMARKS

In this paper, the effectiveness of the SAR image coregistration method accounting for a joint rotation and shift effect designed in [9] has been proved on FOPEN data. The performances have been assessed on the challenging Carabas-II VHF-band FOPEN SAR data demonstrating the effectiveness of the approach for most of the considered rotation angles. Nevertheless, tests have highlighted that increasing further the respective rotation angle between the couple produces a degradation in the registration performances. These results open the way to future developments accounting for also high rotation angles as well as image deformations.

6. REFERENCES

[1] A. Moreira, P. Prats-Iraola, M. Younis, G. Krieger, I. Hajnsek, and K. P. Papathanassiou, "A Tutorial on Synthetic Aperture Radar," *IEEE Geoscience and Remote Sensing Magazine*, vol. 1, no. 1, pp. 6–43, 2013.

[2] Ms P. S. Tondewad and Ms M. P. Dale, "Remote Sensing Image Registration Methodology: Review and Discussion," *Procedia Computer Science*, vol. 171, pp. 2390–2399, 2020.

[3] H. Goncalves, L. Corte-Real, and J. A. Goncalves, "Automatic Image Registration Through Image Segmentation and SIFT," *IEEE Transactions on Geoscience and Remote Sensing*, vol. 49, no. 7, pp. 2589–2600, July 2011.

[4] F. Dellinger, J. Delon, Y. Gousseau, J. Michel, and F. Tupin, "SAR-SIFT: A SIFT-Like Algorithm for SAR Images," *IEEE Transactions on Geoscience and Remote Sensing*, vol. 53, no. 1, pp. 453–466, 2015.

[5] S. Paul and U. C. Pati, "A Block-Based Multifeature Extraction Scheme for SAR Image Registration," *IEEE Geoscience and Remote Sensing Letters*, vol. 15, no. 9, pp. 1387–1391, September 2018.

[6] E. Sansosti, P. Berardino, M. Manunta, F. Serafino, and G. Fornaro, "Geometrical SAR Image Registration," *IEEE Transactions on Geoscience and Remote Sensing*, vol. 44, no. 10, pp. 2861–2870, October 2006.

[7] D. Li and Y. Zhang, "A Fast Offset Estimation Approach for InSAR Image Subpixel Registration," *IEEE Geoscience and Remote Sensing Letters*, vol. 9, no. 2, pp. 267–271, 2011.

[8] L. Pallotta, G. Giunta, and C. Clemente, "Subpixel SAR Image Registration Through Parabolic Interpolation of the 2-D Cross Correlation," *IEEE Transactions on Geoscience and Remote Sensing*, vol. 58, no. 6, pp. 4132–4144, 2020.

[9] L. Pallotta, G. Giunta, C. Clemente, and J. J. Soraghan, "SAR Coregistration by Robust Selection of Extended Targets and Iterative Outlier Cancellation," *IEEE Geoscience and Remote Sensing Letters*, vol. 19, pp. 1–5, 2022.

[10] L. Pallotta, G. Giunta, and C. Clemente, "SAR Image Registration in the Presence of Rotation and Translation: A Constrained Least Squares Approach," *IEEE Geoscience and Remote Sensing Letters*, vol. 18, no. 9, pp. 1595–1599, 2021.

[11] M. Lundberg, L. M. H. Ulander, W. E. Pierson, and A. Gustavsson, "A Challenge Problem for Detection of Targets in Foliage," in *Algorithms for Synthetic Aperture Radar Imagery XIII*. International Society for Optics and Photonics, 2006, vol. 6237, p. 62370K.

[12] K. El-Darymli, P. McGuire, D. Power, and C. R. Moloney, "Target Detection in Synthetic Aperture Radar Imagery: A State-Of-The-Art Survey," *Journal of Applied Remote Sensing*, vol. 7, no. 1, pp. 071598, 2013.

[13] C. Leys, C. Ley, O. Klein, P. Bernard, and L. Licata, "Detecting Outliers: Do not use Standard Deviation Around the Mean, use Absolute Deviation Around the Median," *Journal of Experimental Social Psychology*, vol. 49, no. 4, pp. 764 – 766, 2013.

[14] H. Fitriyah and A. S. Budi, "Outlier Detection in Object Counting based on Hue and Distance Transform using Median Absolute Deviation (MAD)," in *International Conference on Sustainable Information Engineering and Technology (SIET)*. IEEE, 2019, pp. 217–222.